V-type layers are adjoined to the W-type layers. These may correspond to $Yb_6Fe_7O_{19}$ ($n = 6$) or $Yb_7Fe_8O_{22}$ ($n = 7$). A similar intergrowth of these homologous phases was often observed in other grains. It may then be reasonable to consider that such frequent intergrowths have made the accurate X-ray structure analysis of $Yb_3Fe_4O_{10}$ difficult.

References

HORIUCHI, S. & MATSUI, Y. (1974). *Philos. Mag.* **30**, 777–787.

HORIUCHI, S., MATSUI, Y. & BANDO, Y. (1976). *Jpn. J. Appl. Phys.* **15**, 2483–2484.

HORIUCHI, S., MURAMATSU, K. & MATSUI, Y. (1978). *Acta Cryst.* A**34**, 939–946.

KATO, K., KAWADA, I., KIMIZUKA, N. & KATSURA, T. (1975). *Z. Kristallogr.* **141**, 314–320.

KATO, K., KAWADA, I., KIMIZUKA, N., SHINDO, I. & KATSURA, T. (1976). *Z. Kristallogr.* **143**, 278–284.

KIMIZUKA, N., KATO, K., SHINDO, I., KAWADA, I. & KATSURA, T. (1976). *Acta Cryst.* B**32**, 1620–1621.

KIMIZUKA, N. & KATSURA, T. (1975). *J. Solid State Chem.* **15**, 151–157.

SCHERZER, O. (1949). *J. Appl. Phys.* **20**, 20–29.

A Refinement of the Crystal Structure of Monoclinic Europium Sesquioxide*

BY HARRY L. YAKEL

Metals and Ceramics Division, Oak Ridge National Laboratory, PO Box X, Oak Ridge, Tennessee 37830, USA

Abstract

The crystal structure of monoclinic europia (B-Eu_2O_3) was refined by least-squares analyses of Mo $K\alpha$ X-ray scattering data from over 5000 independent reflections. Unit-cell parameters, $a = 14.1105$ (2), $b = 3.6021$ (1), $c = 8.8080$ (2) Å, $\beta = 100.037$ (1)°, were computed from measurements of Bragg angles of reflections with $100° < 2\theta < 163°$. Atom position parameters differ slightly from those reported for B-Sm_2O_3 [Cromer (1957). *J. Phys. Chem.* **61**, 753–755]. There is no clear support for hypotheses that the space group is $C2$ or Cm, rather than $C2/m$. Final measures of agreement were: $R(F^2) = 0.041$, $R_w = 0.065$, and $\sigma_1 = 1.24$ for 4538 reflections with $F_o^2 > \sigma(F_o^2)$. The structure is discussed in terms of the tetrahedrally linked $(MO)_n^{n+}$ layers suggested by Caro [*J. Less-Common Met.* (1968). **16**, 367–377].

Introduction

The monoclinic (B) forms of rare-earth sesquioxides are reportedly stable at temperatures between 1273 and 2273 K for elements near the middle of the lanthanide series (Glushkova, 1965). In a phase diagram they occur between the low-temperature cubic (C) and high-temperature hexagonal (A) phases. A crystal structure for a B-Ln_2O_3 phase was first presented by Cromer (1957), who studied a fragment of B-Sm_2O_3 from a boule melted at 3273–3773 K in an oxyacetylene flame. Atoms were all located in the mirrors of space group $C2/m$; the structure determination and refinement were performed with a few hundred $h0l$ data uncorrected for absorption.

In view of the renewed interest in structural factors affecting the stability and transformation rates of rare-earth oxides, and because the precision of Cromer's results might be improved by detailed analysis of more extensive data, a study of the crystal structure of B-Eu_2O_3 was undertaken.

Experimental

Growth of high-purity B-Eu_2O_3 crystals by convective mass transport from molten NaF has been described by Bennett, Finch, Yakel, Brynestad & Clark (1977). Crystals from this process were preferred for the structural study because (*a*) the growth temperature (1423–1473 K) was in the B-phase stability region, (*b*) the growth could be carried out in dry (<5 p.p.m. H_2O)

argon, and (c) estimates of pertinent impurities (<3 p.p.m. Na, 3 p.p.m. F, 1 p.p.m. Pt) had been obtained.

Preliminary experiments suggested that these crystals are labile to a slow reaction with some component of the ambient laboratory atmosphere, possibly water. A second NaF-flux growth was therefore carried out with the products kept in argon until they could be transferred into a He-filled dry box (<2 p.p.m. H_2O, <6 p.p.m. O_2). In the dry box, a prismatic crystal (27 × 38 × 100 μm) was selected and wedged into a tapered section of a 0·1 mm i.d. thin-walled glass capillary. The capillary was sealed in the dry box with a Pt hot-wire.

X-ray diffraction data were recorded with Mo $K\alpha$ radiation [$\lambda(\alpha_1) = 0.70926$ Å] that was unfiltered for most measurements. The Oak Ridge computer-controlled diffractometer (Busing, Ellison, Levy, King & Roseberry, 1968) was employed for data collection in bisecting geometry for reflections with $2\theta \leq 132°$, and in parallel geometry for reflections with $125° \leq 2\theta \leq 163.4°$. Angular settings centering 77 relatively intense $K\alpha_1$ reflections in the 100–163° 2θ range were entered as observations in a least-squares refinement of

Table 1. *Crystallographic data for B-Eu$_2$O$_3$*

Estimated or least-squares errors in the last significant figure of measured values are given in parentheses.

Molecular weight: 351·92
Crystal system: monoclinic
Probable space group: $C2/m$
Lattice parameters [$T = 294$ (1) K, $\lambda(\alpha_1) = 0.70926$ Å]:

$a = 14.1105$ (2) Å $U = 440.84$ (3) Å^3
$b = 3.6021$ (1) $Z = 6$
$c = 8.8080$ (2) $\rho_x = 7.9536$ (5) Mg m^{-3}
$\beta = 100.037$ (1)°

Linear absorption coefficient: 42·15 mm^{-1}

Table 2. *Conditions of intensity measurements*

Temperature: 294 (1) K
Radiation: Mo $K\alpha(\lambda = 0.71069$ Å)
Take-off angle: 1·2°
Receiving slit: 6 × 6 mm (1·7 × 1·7°)
Scanning mode: θ–2θ steps
Portion of Ewald sphere studied: +h,–k,±l; $h + k = 2n$

	Bisecting (5–132° 2θ)	Parallel (125–163·4° 2θ)
Scan width (2θ)	0·8° + $\alpha_1\alpha_2$ separation	1·2–1·5° (α_1 only)
Step size (2θ)	0·02°	0·02°
Count time/step	2 s (no filter)	4 s (no filter)
	4·5 s (Nb filter)	10 s (Nb filter)
Background count time	100 s (no filter)	120 s (no filter)
	225 s (Nb filter)	300 s (Nb filter)
Standard used (1 : 15 reflections)	11,1,1̄	23,3̄,12
Number of reflections measured (including replicates and standards)	5121	1429
Number of measurements at specified ψ	457	

unit-cell and crystal-orientation parameters. Resultant lattice parameters and other relevant crystallographic data are summarized in Table 1. Experimental conditions used in the collection of diffracted intensity data are given in Table 2.

The mosaic spread of reflections from the crystal studied was typically <0·05° ω. The X-ray take-off angle could, therefore, be reduced to a value (1·2°) that allowed small 2θ scanning ranges without an appreciable increase in statistical counting errors. In parallel diffractometer geometry, the α_1–α_2 resolution was always more than sufficient to allow the α_1 peak alone to be counted. Parallel and bisecting data were brought to the same scale by comparisons of 21 of the more intense reflections in the 125–132° 2θ overlap region.

Typical values of $\sigma(I)/I$, with $\sigma(I)$ based on counting statistics, ranged from <1% for intense reflections to about 10% for weak but definitely observable reflections. After corrections for geometrical and absorption factors, relative F^2 values of moderately intense equivalent reflections in the 0,–k,+l and 0,–k,–l zones agreed to better than 4% on the average. Intensities of Friedel pairs were only measured in the 0,±k,0 and 0,0,±l rows. Differences appeared to be due to large extinction effects rather than to anomalous dispersion in the absence of a symmetry center.

Analysis of the data

Corrections for Lorentz, polarization, and photo-electric-absorption effects were applied to reduce the observed intensity data to relative squares of structure factors. Transmission coefficients were calculated with a modification of the *ORABS* procedure (Wehe, Busing & Levy, 1962); mass absorption coefficients (as well as anomalous-dispersion corrections and atomic-scattering factors for Eu^{3+} and O^{2-}) were taken from *International Tables for X-ray Crystallography* (1974). After elimination of standards, the 6088 observations were condensed to 5222 by averaging replicate measurements; F^2 values for equivalent reflections were not averaged at this stage, since anisotropic extinction effects might be present. Observations were placed on an approximate absolute scale by assuming that all atoms contributed nearly in phase for 0k0 reflections.

Squares of residuals of observed and computed F^2 values were minimized through iterative full-matrix least-squares calculations including all data. Weights, $w_i = 1/\sigma_i^2 = 1/[\sigma_{oi}^2 + (0.03F_i^2)^2]$ were assigned, where σ_{oi}^2 was the variance based on counting statistics. Initial atom position parameters were assumed to be those reported for B-Sm$_2$O$_3$ by Cromer (1957). 14 atomic coordinates, 32 anisotropic thermal vibration parameters, and one overall scale factor were eventually varied for refinements based on $C2/m$.

Table 3. *Indices of agreement for several conditions of refinement*

Definitions of these indices are the standard ones used by crystallographers. See Brown & Chidambaram (1969), for example, for specific equations. Values not in parentheses are computed for all reflections. Values in parentheses are computed for reflections with $F_o^2 > \sigma(F_o^2)$.

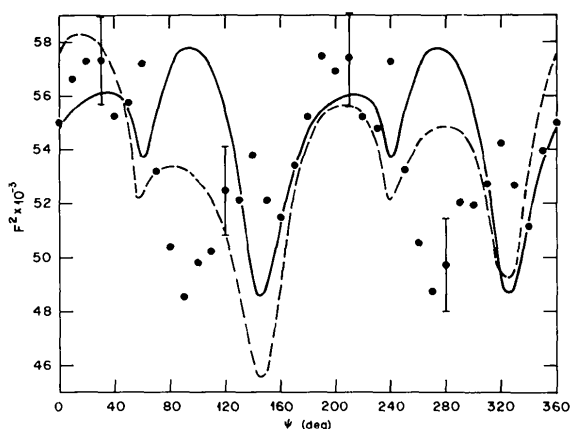| Conditions of refinement	$R(F)$	$R(F^2)$	$R_w(F^2)$	σ_1	Number of observations used	Number of variable parameters
No extinction corrections,	0·0853	0·2326	0·4050	6·13	5222	47
$C2/m$, original data	(0·0760)	(0·2315)	(0·4048)	6·51	4621	47
Isotropic extinction,	0·0515	0·0571	0·0779	1·16	5222	48
$C2/m$, original data	(0·0421)	(0·0560)	(0·0767)	1·21	4621	48
Type I anisotropic	0·0500	0·0504	0·0753	1·12	5222	53
extinction, $C2/m$, original data	(0·0406)	(0·0494)	(0·0740)	1·17	4621	53
Type II anisotropic	0·0491	0·0491	0·0741	1·10	5222	53
extinction, $C2/m$, original data	(0·0399)	(0·0481)	(0·0728)	1·15	4621	53
Type I anisotropic	0·0410	0·0528	0·0740	1·26	5659	53
extinction, $C2/m$, original plus ψ data	(0·0353)	(0·0525)	(0·0731)	1·32	5058	53
Type II anisotropic	0·0426	0·0577	0·0770	1·31	5659	53
extinction, $C2/m$, original plus ψ data	(0·0369)	(0·0574)	(0·0761)	1·37	5058	53
Averaged extinction-	0·0501	0·0510	0·0659	1·18	5118	47
corrected data, $C2/m$	(0·0408)	(0·0500)	(0·0649)	1·24	4538	47
Averaged extinction-	0·0498	0·0510	0·0658	1·18	5118	54
corrected data, $C2$	(0·0404)	(0·0500)	(0·0648)	1·24	4538	54
Averaged extinction-	0·0492	0·0506	0·0648	1·17	5118	89
corrected data, Cm	(0·0392)	(0·0494)	(0·0636)	1·22	4538	89

Fig. 1. Variations of observed and computed values of F^2 with angle of rotation, ψ, about the $0\bar{2}0$ diffraction vector. Observed values have been corrected for all physical effects save extinction, and are shown as points, with error bars attached to some. Computed values for type I and type II anisotropic extinction models are shown as continuous and dashed curves, respectively.

As anticipated, extinction effects proved large. Introduction of the secondary-extinction corrections defined by Zachariasen (1967) and Coppens & Hamilton (1970) gave statistically significant improvements in standard measures of agreement (see Table 3). In an attempt to discriminate between the abilities of

Table 4. *Positional parameters for B-Eu_2O_3 (C2/m)*

Least-squares standard errors in the last significant figure are given in parentheses. Fixed values have no error indicated.

	x	y	z
Eu(1)	0·13740 (1)	$\frac{1}{4}$	0·4897 (2)
Eu(2)	0·18972 (1)	$\frac{1}{4}$	0·13760 (2)
Eu(3)	0·46635 (1)	$\frac{1}{4}$	0·18763 (2)
O(1)	0·1291 (2)	0	0·2855 (3)
O(2)	0·3248 (2)	$\frac{1}{4}$	0·0267 (3)
O(3)	0·2961 (3)	$\frac{1}{4}$	0·3732 (4)
O(4)	0·4734 (2)	0	0·3431 (3)
O(5)	0	$\frac{1}{4}$	0

type I and type II anisotropic corrections to match the extinction effects present in the data from this crystal, intensities of 14 accessible reflections with probable extinction correction factors between 0·25 and 0·57 were measured at increments of 10° about their diffraction vectors (ψ axis), except for gaps where instrumental interference occurred. A total of 437 observations, exclusive of standards, were added to the original data set, and least-squares solutions for anisotropic extinction parameters were recomputed. Results summarized in Table 3 showed that the overall fit with type I parameters (mean mosaic-spread parameter $\eta = 3''$) might be superior to that with type II parameters (mean domain radius $r = 2$ μm). However, as may be seen in Fig. 1, neither extinction model was able to

satisfactorily reproduce the observed variations of F^2 with ψ for a typical extinction-affected reflection such as $0\bar{2}0$ (correction factor $= 0.25$).

Despite these evident disagreements, corrections based on an assumed type I anisotropic extinction model were computed and applied to all 5659 observed data. Equivalents were then averaged to yield a final set of 5118 data corrected for all physical effects including extinction. Final indices of agreement from least-squares cycles based on this data set and a centrosymmetric structure appear in Table 3. Atom position parameters are given in Table 4.*

The symmetry of the structure was then lowered by displacing one Eu ion in order to eliminate in turn the mirrors and the twofold axes. Table 3 again summarizes agreement measures produced by least-squares

---

* Lists of structure factors and anisotropic thermal parameters have been deposited with the British Library Lending Division as Supplementary Publication No. SUP 34098 (28 pp.). Copies may be obtained through The Executive Secretary, International Union of Crystallography, 5 Abbey Square, Chester CH1 2HU, England.

fits to the respective $C2$ and Cm models. While R factor ratio tests (Hamilton, 1965) could be rigidly interpreted to show that the Cm structure is statistically preferable to the centrosymmetric solution, uncertainties as to the adequacy of the extinction corrections dictate the more cautious conclusion that a non-centrosymmetric structure is possible but not proved.

A difference Fourier map based on the results of the final least-squares cycle for the centrosymmetric structure showed positive and negative peaks corresponding to an electron density of about ± 0.6 e Å^{-3} in diffraction ripples near Eu ions. These were the only significant features of the map.

Discussion

Coordinates listed in Table 4 differ only slightly from those for $B\text{-Sm}_2\text{O}_3$ (Cromer, 1957), but have a precision an order of magnitude greater. Thermal vibration parameters are also better defined and show a different

Table 5. *Interionic distances (Å) and angles (°) in B-Eu_2O_3 ($C2/m$)*

Estimated standard deviations in the last significant figure are given in parentheses. The number of symmetrically equivalent distances or angles is given, if more than one, in square brackets. The atom-labeling scheme corresponds to that used in Fig. 2.

Europium environments

(a) Europium—oxygen distances

Eu(1)–O(3)	2·290 (2) [2]	Eu(1)–O(1)	2·537 (2) [2]
–O(4)	2·297 (3)	–O(3)	2·656 (4)
–O(4)	2·414 (3)		
Eu(2)–O(2)	2·288 (2)	Eu(2)–O(1)	2·462 (2) [2]
–O(2)	2·297 (2) [2]	–O(5)	2·7394 (2)
–O(3)	2·340 (3)		
Eu(3)–O(2)	2·239 (2)	Eu(3)–O(5)	2·5444 (1) [2]
–O(4)	2·254 (2) [2]	–O(3)	3·133 (4)
–O(1)	2·308 (3)		

(b) Oxygen—oxygen distances

About Eu(1)

O(4)–O(4)	2·735 (5)	O(4)–O(3)	3·131 (4) [2]
O(4)–O(1)	2·952 (3) [2]	O(3)–O(3)	3·307 (7) [2]
O(3)–O(1)	2·960 (3) [2]	O(1)–O(1')	3·6021 (1)
O(3)–O(1)	3·007 (4) [2]	O(3)–O(3')	3·6021 (1)

About Eu(2)

O(2)–O(2)	2·751 (4) [2]	O(3)–O(2)	3·148 (4)
O(1)–O(2)	2·935 (4) [2]	O(5)–O(1)	3·360 (2) [2]
O(3)–O(1)	2·960 (3) [2]	O(1)–O(1')	3·6021 (1)
O(5)–O(2)	3·101 (2) [2]	O(2)–O(2')	3·6021 (1)

About Eu(3)

O(1)–O(4)	2·952 (3) [2]	O(1)–O(5)	3·360 (2) [2]
O(2)–O(5)	3·101 (2) [2]	O(4)–O(4')	3·6021 (1)
O(4)–O(5)	3·110 (3) [2]	O(5)–O(5')	3·6021 (1)
O(3)–O(4)	3·131 (4) [2]	O(2)–O(4)	3·656 (3) [2]
O(3)–O(2)	3·148 (4)		

Oxygen environments

(a) Europium—oxygen—europium angles

About O(2)

Eu(3), Eu(2)	116·6 (1)	Eu(2), Eu(2)	106·25 (7) [2]
Eu(3), Eu(2)	111·74 (7) [2]	Eu(2), Eu(2')	103·3 (1)

About O(3)

Eu(1), Eu(1')	103·7 (1)	Eu(2), Eu(1)	83·2 (1)
Eu(1), Eu(2)	128·05 (6)[2]	Eu(2), Eu(3)	88·2 (1)
Eu(1), Eu(1)	96·4 (1) [2]	Eu(1), Eu(3)	171·4 (1)
Eu(1), Eu(3)	88·8 (1) [2]		

About O(4)

Eu(3), Eu(3')	106·1 (1)	Eu(3), Eu(1)	105·22 (7) [2]
Eu(3), Eu(1)	115·19 (7) [2]	Eu(1), Eu(1)	109·1 (1)

(b) Europium—europium distances

About O(1)

Eu(1)–Eu(2)	3·3257 (2) [2]	Eu(1)–Eu(3)	3·7099 (2) [2]
Eu(1)–Eu(1')	3·6021 (1)	Eu(2)–Eu(3)	3·7224 (2) [2]
Eu(2)–Eu(2')	3·6021 (1)		

About O(2)

Eu(2)–Eu(2')	3·6021 (1)	Eu(3)–Eu(2)	3·7551 (2) [2]
Eu(2)–Eu(2)	3·6676 (2) [2]	Eu(3)–Eu(2)	3·8511 (2)

About O(3)

Eu(2)–Eu(1)	3·3257 (2)	Eu(3)–Eu(1)	3·8427 (2) [2]
Eu(1)–Eu(1')	3·6021 (1)	Eu(3)–Eu(2)	3·8511 (2)
Eu(1)–Eu(1)	3·6957 (3) [2]	Eu(2)–Eu(1)	4·1620 (2) [2]

About O(4)

Eu(3)–Eu(3')	3·6021 (1)	Eu(1)–Eu(1)	3·8372 (3)
Eu(1)–Eu(3)	3·7099 (2) [2]	Eu(1)–Eu(3)	3·8427 (2) [2]

About O(5)

Eu(3)–Eu(3)	3·5946 (4) [2]	Eu(2)–Eu(3)	3·7224 (2) [4]
Eu(3)–Eu(3')	3·6021 (1) [2]	Eu(2)–Eu(3)	3·7551 (2) [4]

and more structurally reasonable pattern than those reported for the samarium analogue. The r.m.s. displacements of the O(5) ion are slightly greater than those for O(1), O(2), and O(4), but do not approach the relatively large value for the corresponding ion in B-Sm_2O_3. On the other hand, the major displacement of the O(3) ion is half as large again as that of any other O ion in monoclinic europia, whereas the isotropic B value of O(3) in monoclinic samaria is the smallest of all atoms in the structure.

Near-neighbor interionic distances are summarized in Table 5; atom designators are those used in the drawings of these environments presented in Fig. 2. Interionic angles about O(2), O(3), and O(4) are included in Table 5, since they are of special interest in the following discussion. Idealized sevenfold anion coordination polyhedra about Eu ions have the previously noted forms, viz, trigonal prisms with a seventh O at a slightly larger distance along a prism face normal [Eu(1) and Eu(2)], and octahedra with a seventh O at a substantially larger distance along an approximate octahedral face normal [Eu(3)]. The distances listed in Table 5 are not too different from those reported for B-Sm_2O_3, provided a few errors in the latter tabulation are corrected.

If the overall structure of monoclinic rare-earth sesquioxides is viewed in terms of anion coordinations about cations, a complex picture emerges that does little to explain either the stability of the B-phase or its relationships to the A and C forms. Caro (1968)

pointed out that, given the radii of the ions involved, a view stressing cation coordinations about anions is not only reasonable but also leads to an appreciation of structural similarities among the phases. In this approach, tetrahedral OM_4 linkages share edges to build $(MO)_n^{n+}$ sheets that are discernible in A and B forms, and, allowing for interpenetration, in the C form. Specifically the O(2), O(3) and O(4) ions are represented as lying within such sheets, and as having tetrahedral cation environments, while the O(1) and O(5) ions lie between sheets and have distorted square-pyramidal and octahedral cation coordinations.

A drawing of the refined B-Eu_2O_3 structure that emphasizes Caro's proposed cationic $(EuO)_n^{n+}$ sheets is presented in Fig. 3; cation environments of the five crystallographically distinct O ions are displayed in Fig. 2(d–h). One sees that the coordination polyhedra of only O(2) and O(4) approach ideal tetrahedra, but that the polyhedron about O(3) is more nearly a planar triangle, the longer Eu(1) and Eu(3) contacts completing an irregular trigonal bipyramid. Furthermore, the extremely long O(3)—Eu(3) contact (3·13 Å) lies within a cationic sheet, while the shorter O(3)—Eu($\underline{1}$) contact (2·66 Å) bridges the gap between sheets. The claim that, of the seven M—O contacts about each rare-earth ion in the B-phase structure, four short contacts lie within cationic sheets and three long contacts lie between them must also be amended for the octahedrally coordinated Eu ion.

Aside from the oversimplifications emerging from comparisons of the actual refined structure of B-Eu_2O_3 and Caro's model, the unifying features of that model should not be ignored. Lejus, le Bernier & Collongues (1976) have reported observations on the initial stages of hydration of B-Eu_2O_3 crystals, which they interpret by envisioning penetration of water into the crystal between the $(EuO)_n^{n+}$ layers. Tests of this mechanism could be made by deliberately exposing the isolated crystal studied in the present experiment to a humid atmosphere.
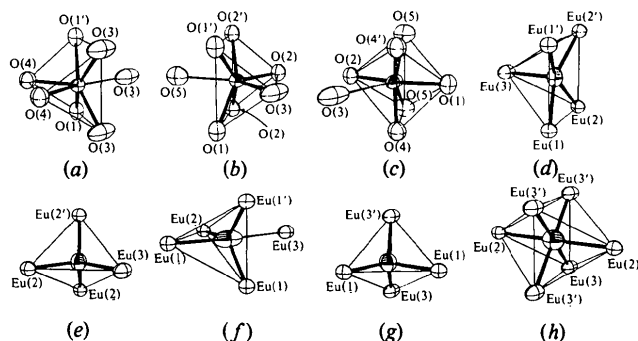

Fig. 2. (a–c) Environments of europium ions Eu(1), Eu(2), Eu(3). The plane containing **b** and **c** is normal to the page and its trace is vertical. The **b** axis points up from the page at an angle of 16°. Thick Eu—O bonds connect ions separated by less than 2·6 Å; thinner Eu—O bonds connect ions separated by 2·6–3·2 Å. Thin O—O stick bonds outline the primary anion coordination polyhedron about each europium ion. (d–h) Environments of oxygen ions O(1)—O(5). The **a** axis is in the plane of the page and points horizontally to the right. The **b** axis points up from the page at an angle of 16°. Thick O—Eu bonds connect ions separated by less than 3 Å; a thinner bond connects O(3) and Eu(3) separated by 3·13 Å. Thin Eu—Eu stick bonds outline the primary cation coordination polyhedron about each O ion. All drawings have the same scale, and all ions are represented by thermal vibration ellipsoids including 99·9% probability (Johnson, 1976).
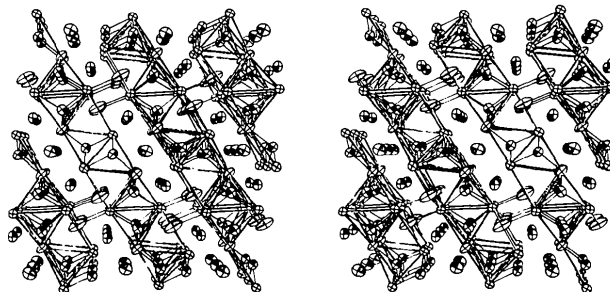

Fig. 3. Stereoview of the crystal structure of monoclinic Eu_2O_3 viewed along the **b** axis with **a** horizontal and pointing to the right. Coordination polyhedra of Eu ions about O(2), O(3), and O(4) are outlined by stick bonds so as to emphasize the $(EuO)_n^{n+}$ sheets. O(3)—Eu($\underline{1}$) contacts that bridge the gaps between sheets are indicated as thin stick bonds. Polyhedra about O(1) and O(5) are omitted for purposes of clarity.

I am indebted to Drs C. B. Finch and S. L. Bennett of the Metals and Ceramics Division, Oak Ridge National Laboratory, who grew the crystals used in this work. Thanks are also due to Drs W. R. Busing and H. A. Levy of the Chemistry Division, Oak Ridge National Laboratory, who made their computer-controlled diffractometer available for the data collection.

References

BENNETT, S. L., FINCH, C. B., YAKEL, H. L., BRYNESTAD, J. & CLARK, G. W. (1977). *J. Cryst. Growth,* **41**, 309–310.
BROWN, G. M. & CHIDAMBARAM, R. (1969). *Acta Cryst.* B**25**, 676–687.
BUSING, W. R., ELLISON, R. D., LEVY, H. A., KING, S. P. & ROSEBERRY, R. T. (1968). *The Oak Ridge Computer-Controlled Diffractometer.* Report ORNL-4143. Oak Ridge National Laboratory, Tennessee.

CARO, P. E. (1968). *J. Less-Common Met.* **16**, 367–377.
COPPENS, P. & HAMILTON, W. C. (1970). *Acta Cryst.* A**26**, 71–83.
CROMER, D. T. (1957). *J. Phys. Chem.* **61**, 753–755.
GLUSHKOVA, V. B. (1965). *Polymorphism of Rare-Earth Oxides.* Leningrad: Nauka.
HAMILTON, W. C. (1965). *Acta Cryst.* **18**, 502–510.
International Tables for X-ray Crystallography (1974). Vol. IV, pp. 61–68, 72–78, 149–150. Birmingham: Kynoch Press.
JOHNSON, C. K. (1976). *ORTEP* II. Report ORNL-5138. Oak Ridge National Laboratory, Tennessee.
LEJUS, A.-M., LE BERNIER, J.-C. & COLLONGUES, R. (1976). *Rev. Int. Hautes Temp. Refract.* **13**, 25–29.
WEHE, D. J., BUSING, W. R. & LEVY, H. A. (1962). *ORABS.* Report ORNL-TM-229. Oak Ridge National Laboratory, Tennessee.
ZACHARIASEN, W. H. (1967). *Acta Cryst.* **23**, 558–564.

Structure du Dichlorure de Cadmium Tétrahydraté

PAR H. LELIGNY ET J. C. MONIER

Laboratoire de Cristallographie et Chimie du Solide, associé au CNRS n° 251, Laboratoire de Cristallographie-Minéralogie, UER des Sciences, Université, 14032 Caen CEDEX, France

Abstract

$CdCl_2.4H_2O$ crystallizes in the orthorhombic system with space group $P2_12_12_1$. The unit-cell dimensions are $a = 12.889$ (2), $b = 7.281$ (1), $c = 15.010$ (8) Å; $Z = 8$, $d_c = 2.409$ Mg m^{-3}. The structure was refined to a final R of 0.051 ($R_w = 0.057$) for 1967 independent reflections registered with an automatic four-circle diffractometer at 247 (1) K. The Cd atoms are octahedrally coordinated to four Cl and two O atoms. The crystal structure consists of individual chains of octahedra packed along [001] with two shared Cl—Cl edges. These chains are linked by hydrogen bonds.

Introduction

Dans le cadre d'une étude concernant les sels hydratés, nous avons entrepris la détermination de la structure relative au chlorure de cadmium à $4H_2O$ après avoir résolu celles de $CdCl_2.H_2O$ et $CdCl_2.2,5H_2O$ (Leligny & Monier, 1974, 1975).

Les cristaux de $CdCl_2.4H_2O$ s'obtiennent à partir d'une solution aqueuse de chlorure de cadmium maintenue au voisinage de 273 K. Ils sont légèrement allongés selon [001]; leur faciès comporte des prismes $\{hk0\}$ et $\{h0l\}$ accompagnant le pinacoïde $\{100\}$ qui est la forme la plus développée.

Les clichés réalisés à l'aide de chambres de Weissenberg et de Buerger à température proche de 273 K nous ont permis d'établir que $CdCl_2.4H_2O$ cristallise dans le groupe $P2_12_12_1$ et que ses paramètres présentent une relation simple avec ceux de $CdBr_2.4H_2O$ (Leligny & Monier, 1978): a et b sont pratiquement les mêmes alors que le paramètre c vaut approximativement quatre fois celui du bromure.

Les diagrammes de diffraction montrent que les réflexions hkl se répartissent en trois ensembles, $l = 4n$ de fortes intensités, $l = 2n + 1$ d'intensités moindres, $l = 4n + 2$ de très faibles intensités.

Enregistrement des intensités

L'enregistrement du spectre de diffraction a été réalisé sur un diffractomètre CAD-4 Enraf–Nonius avec la radiation $K\bar{\alpha}$ du molybdène isolée par un monochromateur à lame de graphite. Le cristal utilisé,